

Spatial and temporal propagation of Kondo correlations

Benedikt Lechtenberg and Frithjof B. Anders

Lehrstuhl für Theoretische Physik II, Technische Universität Dortmund, 44221 Dortmund, Germany

(Dated: December 6, 2024)

We address the fundamental question how the spatial Kondo correlation are building up in time assuming an initially decoupled impurity spin \vec{S}_{imp} . We investigate the time-dependent spin-correlation function $\chi(\vec{r}, t) = \langle \vec{S}_{\text{imp}} \vec{s}(\vec{r}) \rangle(t)$ in the Kondo model with antiferromagnetic and ferromagnetic coupling where $\vec{s}(\vec{r})$ denotes the spin density of the conduction electrons after switching on the Kondo coupling at time $t = 0$. We present data obtained from a time-dependent numerical renormalisation group (TD-NRG) calculation. We gauge the accuracy of our two-band NRG by the spatial sum-rules of the equilibrium correlations functions and the reproduction of the analytically exactly known spin-correlation function of the decoupled Fermi sea. We find a remarkable building up of Kondo-correlation outside of the light-cone defined by the Fermi velocity of the host metal. By employing a perturbative approach exact in second-order of the Kondo coupling, we connect these surprising correlations to the intrinsic spin-density entanglement of the Fermi sea.

PACS numbers: 03.65.Yz, 73.21.La, 73.63.Kv, 76.20.+q

I. INTRODUCTION

A localized spin interacting antiferromagnetically with a metallic host is one of the fundamental problems in theoretical condensed matter physics. Originally proposed by Kondo [1] for understanding the low-temperature resistivity [2] in gold wires containing a low concentration Cu impurities, it has also been realised by depositing magnetic ad-atoms [3–5] or molecules on metallic surfaces. Scanning tunneling microscopes (STM) allow to manipulate and detect magnetic ad-atoms on metallic substrates using the Kondo resonance [1]. Quantum corrals have been build and coherent interference of the electrons were detected on the substrate surfaces using STM [3–5]. In 1998, David Goldhaber-Gordon demonstrated in a seminal paper [6] that the Kondo effect can also be observed in single-electron transistors [7] realised by a semiconductor quantum dot. Both types of experiments have opened up a new field of observing the Kondo-effect in nano-devices [8–10].

While the equilibrium properties of the Kondo problem are theoretically well understood by the virtue of Wilson’s numerical renormalization group (NRG) [11, 12] approach and the exact Bethe ansatz solution [13], its non-equilibrium properties are subject to active research [14–22].

In this paper, we address the fundamental question how the spatial Kondo correlation are building up in time assuming an initially decoupled impurity spin \vec{S}_{imp} . We have investigated the time-dependent spin-correlation function $\chi(\vec{r}, t) = \langle \vec{S}_{\text{imp}} \vec{s}(\vec{r}) \rangle(t)$ using the time-dependent NRG (TD-NRG) [17]. $\vec{s}(\vec{r})$ denotes the spin density of the conduction electrons at distance $R = |\vec{r}|$ from the impurity after switching on the Kondo-coupling at time $t = 0$. Since the spins are initially uncorrelated, this correlation function vanishes for $t \leq 0$ and is a measure of the building up of the spatial entanglement between the local spin and the conduction-electron spin density.

For infinitely long times, the equilibrium spatial cor-

relation function of the Kondo model must be recovered. This correlation function $\chi_{\infty}(\vec{r}) = \lim_{t \rightarrow \infty} \chi(\vec{r}, t)$ has been investigated intensively by Affleck and collaborators [23–26] using fieldtheoretical methods in the last 15 years. It accounts for alternating ferromagnetic and anti-ferromagnetic correlations as expected by spin-correlations mediated by the RKKY mechanism. Furthermore, the crossover between different power-law decays for short and long distances, found [27] in $\chi_{\infty}(\vec{r})$, occurs at a characteristic length scale $\xi_K = v_F/T_K$ which has been interpreted as size of the Kondo screening cloud [23–26, 28], where v_F being the Fermi velocity, and T_K the Kondo temperature governing the crossover from a free impurity spin at high temperatures to the singlet formation for $T \rightarrow 0$. Therefore, the two limits, $t = 0$ and $t = \infty$, are known and used as reference points for our calculations.

The time-dependent spin-correlation function $\chi(\vec{r}, t)$ contains the information about how the spin correlations propagate through the system. We have found for an antiferromagnetic Kondo coupling (i) ferromagnetic correlations propagating away from the impurity with the Fermi-velocity v_F , which defines the “light-cone” [29] of the problem, and (ii) in addition finite and non-exponential small correlations outside of this light-cone. We have been able (iii) to trace back the response outside of the light-cone to the intrinsic entanglement of the Fermi sea using a controlled second-order expansion in the Kondo coupling constant and comparing the perturbative results with the full TD-NRG simulation. Since $\chi(\vec{r}, t)$ is not a response function, correlations outside of the light-cone are allowed. Any response function, however, describing the transmission of signals vanishes outside of the light-cone in accordance with relativity [22].

Our TD-NRG results agree remarkably well with our perturbative theory for short and intermediate time and length scales and approach the correct equilibrium correlation functions in the long-time limit. Our data confirm the recent findings by Medvedyeva *et al.* [22] but

also considerably extend their work: we include the full spatial dependence which allows us to access the full $2k_F$ oscillations inherent to the RKKY mediated correlations. Furthermore, the crossover between short and long distances, i. e. $R \ll \xi_K$ and $R \gg \xi_K$, including the Kondo physics at low temperature in the strong coupling regime is fully accessible by the NRG which cannot be revealed by perturbative approaches.

Borda has pioneered the calculation of equilibrium spatial correlation function for the Kondo model using the NRG [27]. He has realized that this problem is equivalent to the two-impurity Kondo model [30–32] where the second impurity spin has been removed while the local conduction electron density operator $\vec{s}(\vec{r})$ is used as a probe for the spin correlations. By mapping the problem onto two \vec{r} -dependent linear combinations of conduction electrons with even and odd symmetry under spatial inversion around the mid-point $\vec{r}/2$, the calculation of spatial correlations become accessible to the NRG. Thereby, the spatial information [27, 31–33] is encoded in the energy dependent density of states (DOS) of the even and odd bands. Since a single two-band NRG run is required for each distance R , the numerical calculations are very involved and require an independent NRG calculation with individually adapted bands for each distance R .

In this paper, we use an improved mapping compared to Borda's original work [27]. Our modifications are able (i) to accurately reproduce the analytically known sum-rules [23, 27, 28] for the spin-correlation function in the ferromagnetic and antiferromagnetic Kondo regime, (ii) reproduce the analytical spin-spin correlation function of the decoupled Fermi sea exactly, and (iii) obtain sign changes $\chi_\infty(\vec{r})$ at short and intermediate distances expected from RKKY mediated correlations. While Borda reported [27] that $\chi_\infty(\vec{r})$ remains negative for all distances and Kondo couplings as can be seen in Fig. 2 of Ref. 27, we find oscillating and power-law decaying $\chi_\infty(\vec{r}) < 0$ only for distances $R \gg \xi_K$ in accordance with previous analytic predictions using a 1D field theoretical approach [23, 28]. At short distances, the Kondo screening is incomplete and, therefore, alternating signs are found in $\chi_\infty(\vec{r})$.

A. Plan of the Paper

The paper is organised as follows. We begin with the definition of the model in Sec. II A and derive the mapping to the two-impurity model in Sec. II B. After that we discuss in Sec. II C the exact sum-rules of the equilibrium spin-correlation function for the Kondo regime and the local moment regime relevant for a ferromagnetic Kondo coupling.

In Secion III, we present our equilibrium results for $\chi_\infty(R)$ for ferromagnetic and antiferromagnetic couplings which differ slightly from the previously reported data by Borda [27] and discuss the effect of spatial dimensions.

In Secion IV A, we provide a short summary of the TD-NRG employed in the following to obtain the non-equilibrium quench dynamics. Secion IV B is devoted to our numerical TD-NRG data on the temporal buildup of the spatial Kondo correlations. In order to understand the surprising buildup of the Kondo correlations outside of the light-cone, a second-order perturbative calculation presented in Sec. IV C is able to provide an analytical explanation of the origin of this unusual correlations found in the TD-NRG. We use these analytical results to also explain the spatial and temporal building up of spin-correlation for ferromagnetic couplings in Sec. IV E. We conclude with a summary and outlook.

II. THEORY

A. Definition of the model

We investigate the spatial and temporal correlation between the conduction electron spin density $\vec{s}(\vec{r})$ and a localized impurity spin \vec{S}_{imp} coupled locally to the metallic host via Kondo interaction [1]. For a generic system, we can neglect the details of the atomic wave function and expand the spin-density operator $\vec{s}(\vec{r})$ in plane waves [34]

$$\vec{s}(\vec{r}) = \frac{1}{2} \frac{1}{NV_u} \sum_{\sigma\sigma'} \sum_{\vec{k}\vec{k}'} c_{\vec{k}\sigma}^\dagger [\vec{\sigma}]_{\sigma\sigma'} c_{\vec{k}'\sigma'} e^{i(\vec{k}' - \vec{k})\vec{r}} \quad (1)$$

where N is the number of unit cells in the Volume V , $V_u = V/N$ is the volume of the unit cell, and \vec{k} the momentum vector. In an energy representation [11, 34], the Kondo Hamiltonian [1] of the system

$$H = H_0 + H_K \quad (2)$$

$$H_0 = \sum_{\sigma} \int_{-D}^D d\varepsilon \varepsilon c_{\varepsilon\sigma}^\dagger c_{\varepsilon\sigma}$$

$$H_K = J \vec{S}_{\text{imp}} \vec{s}_c(0)$$

describes this local impurity spin located at the origin coupled via an effective Heisenberg coupling to the unit cell volume averaged conduction electron spin $\vec{s}_c(\vec{r}) = V_u \vec{s}(\vec{r})$ with a coupling constant J ; H_0 accounts for the energy of the free conduction electrons.

Wilson [11, 12] realized that the logarithmic divergencies generated by a perturbative treatment [1] of the Kondo coupling can be circumvented by discretizing the energy spectrum of the conduction band on a logarithmic grid [11] using a dimensionless discretization parameter $\Lambda > 1$. Consequently, all intervals contribute equally to the divergence and the problem can be solved by iteratively adding these intervals with progressively smaller energy. The continuum limit is recovered for $\Lambda \rightarrow 1$. Using an appropriate unitary transformation [11], the Hamiltonian is mapped onto a semi-infinite chain, with the impurity coupled to the first chain site. The N th link along the chain represents an exponentially deca-

ing energy scale: $D_N \sim \Lambda^{-N/2}$. Using this hierarchy of scales, the sequence of finite-size Hamiltonians \mathcal{H}_N for the N -site chain is solved iteratively, discarding the high-energy states at the conclusion of each step to maintain a manageable number of states. The reduced basis set of \mathcal{H}_N so obtained is expected to faithfully describe the spectrum of the full Hamiltonian on a scale of D_N , corresponding to the temperature $T_N \sim D_N$. Details can be found in the review [12] on the NRG by Bulla et al.

B. Spatial correlations

While Wilson's original approach was tailored towards solving the thermodynamics of local impurity and classifying the fixed points of the Hamiltonian, we are explicitly interested in the time evolution of the spatial spin-correlation functions $\langle \vec{S}_{\text{imp}} \vec{s}(\vec{r}) \rangle(t)$ at the distances R . For a rotational invariant system considered here, this quantity is isotropic and only dependent on R . The correlations between those spatially well separated points are mediated by the conduction electrons which is linked to the RKKY interaction.

Borda has realized [27] that the calculation of the spatial correlations is related to a simplified two-impurity problem. Originally Jones et al. [31, 32] have extended the NRG [11] to a two-impurity Kondo model,

$$H = H_0 + \sum_{i=\pm} J_i \vec{S}_{\text{imp}}^i \vec{s}_c(\vec{R}_i), \quad (3)$$

where the two impurity spins \vec{S}_{imp}^i are located at the position $\vec{R}_{\pm} = \pm \vec{r}/2$ and coupled to the same conduction band. The spatial dependency is included into the two non-orthogonal energy-dependent field operators

$$c_{\varepsilon\sigma,\pm} = \frac{1}{\sqrt{N\rho(\varepsilon)}} \sum_{\vec{k}} \delta(\varepsilon - \varepsilon_{\vec{k}}) c_{\vec{k}\sigma} e^{\pm i\vec{k}\vec{r}/2} \quad (4)$$

which are combined to even (e) and odd (o) parity eigenstates [30–33]

$$\begin{aligned} c_{\varepsilon\sigma,e} &= \frac{1}{N_e(\varepsilon)} (c_{\varepsilon\sigma,+} + c_{\varepsilon\sigma,-}) \\ c_{\varepsilon\sigma,o} &= \frac{1}{N_o(\varepsilon)} (c_{\varepsilon\sigma,+} - c_{\varepsilon\sigma,-}) \end{aligned} \quad (5)$$

of H_0 . The dimensionless normalization functions $N_{e(o)}(\varepsilon)$

$$\begin{aligned} N_e^2(\varepsilon) &= \frac{4}{N\rho(\varepsilon)} \sum_{\vec{k}} \delta(\varepsilon - \varepsilon_{\vec{k}}) \cos^2\left(\frac{\vec{k}\vec{r}}{2}\right) \\ N_o^2(\varepsilon) &= \frac{4}{N\rho(\varepsilon)} \sum_{\vec{k}} \delta(\varepsilon - \varepsilon_{\vec{k}}) \sin^2\left(\frac{\vec{k}\vec{r}}{2}\right) \end{aligned} \quad (6)$$

are computed from the anti-commutation relation $\{c_{\varepsilon\sigma,\alpha}, c_{\varepsilon\sigma,\alpha'}^\dagger\} = \delta(\varepsilon - \varepsilon') \delta_{\alpha\alpha'} \delta_{\sigma\sigma'}$. Note that both densi-

ties $N_e(\varepsilon)$ and $N_o(\varepsilon)$ depend on the distance $R = |\vec{r}|$ and are not normalized. $\rho(\varepsilon)$ denotes the conduction band density of states of the original band.

The two-impurity Hamiltonian (3) can be written in terms of these even and odd fields and solved using the NRG [31, 32]. By omitting one of the two-impurity spins [27], i. e. \vec{S}_{imp}^- , the original Kondo Hamiltonian (2) is recovered for an impurity spin located at \vec{R}_+ . Furthermore, $\vec{s}_c(\vec{R}_-)$ can be used for probing the isotropic spin-correlation function $\langle \vec{S}_{\text{imp}} \vec{s}(\vec{r}) \rangle$.

The local even or odd parity conduction electron operators coupling to the impurity spin take the form

$$f_{0\sigma,e(o)} = \frac{1}{\bar{N}_{e(o)}} \int d\varepsilon \sqrt{\rho(\varepsilon)} N_{e(o)}(\varepsilon) c_{\varepsilon\sigma,e(o)}, \quad (7)$$

and its anti-commutator $\{f_{0\sigma,e(o)}, f_{0\sigma',e(o)}^\dagger\} = \delta_{\sigma\sigma'}$ determines the dimensionless normalization constants

$$\bar{N}_{e(o)} = \left[\int d\varepsilon N_{e(o)}^2(\varepsilon) \rho(\varepsilon) \right]^{1/2}. \quad (8)$$

These constants enter the definition of the effective parity density of states

$$\rho_{e(o)}(\varepsilon) = \frac{1}{\bar{N}_{e(o)}^2} N_{e(o)}^2(\varepsilon) \rho(\varepsilon) \quad (9)$$

which accounts for the position dependency and are used in the construction of the NRG tight-binding chain - for details see the NRG review in Ref. [12].

Then, the original Kondo Hamiltonian (2) is expanded in these orthogonal even and odd fields

$$\begin{aligned} H &= \sum_{\sigma} \sum_{\alpha=e,o} \int_{-D}^D d\varepsilon \varepsilon c_{\varepsilon\sigma,\alpha}^\dagger c_{\varepsilon\sigma,\alpha} \\ &+ \frac{J}{8} \sum_{\sigma\sigma'} \left(\bar{N}_e f_{0\sigma,e}^\dagger + \bar{N}_o f_{0\sigma,o}^\dagger \right) [\underline{\vec{s}}]_{\sigma\sigma'} \\ &\times \left(\bar{N}_e f_{0\sigma,e} + \bar{N}_o f_{0\sigma,o} \right) \vec{S}_{\text{imp}} \end{aligned} \quad (10)$$

after positioning the impurity spin at \vec{R}_+ . The spin-density operator at \vec{R}_- entering the spatial correlation function is given by

$$\begin{aligned} \vec{s}(\vec{R}_-) &= \frac{1}{8V_u} \sum_{\sigma\sigma'} \left(\bar{N}_e f_{0\sigma,e}^\dagger - \bar{N}_o f_{0\sigma,o}^\dagger \right) [\underline{\vec{s}}]_{\sigma\sigma'} \\ &\times \left(\bar{N}_e f_{0\sigma,e} - \bar{N}_o f_{0\sigma,o} \right) \end{aligned} \quad (11)$$

where V_u accounts for its dimensions. Note the inclusion of the proper R -dependent normalization constants \bar{N}_e, \bar{N}_o into the Hamiltonian and the spin-density operator $\vec{s}(\vec{R}_-)$ which are crucial for recovering the exact sum-rules discussed in the following section.

C. Sum-rule of the spatial correlation function

The quality of the calculated spatial correlation function can be verified by a sum-rule derived for the strong-coupling fixed point at $T = 0$. Since the ground state $|0\rangle$ is a singlet in the Kondo-regime, the application of the total spin operator of the system comprising local and total conduction electron spin

$$\vec{S}_{\text{tot}}|0\rangle = \left(\vec{S}_{\text{imp}} + \int s(\vec{r}) d^D r \right) |0\rangle = 0 \quad (12)$$

must vanish. Consequently the correlator $\langle 0 | \vec{S}_{\text{imp}} \vec{S}_{\text{tot}} | 0 \rangle$ also vanishes,

$$\langle 0 | \vec{S}_{\text{imp}} \vec{S}_{\text{tot}} | 0 \rangle = \frac{3}{4} + \int \langle 0 | \vec{S}_{\text{imp}} \vec{s}(\vec{r}) | 0 \rangle d^D r = 0, \quad (13)$$

and, therefore, $\chi_\infty(r)$ must obey the sum rule:

$$\int \langle \vec{S}_{\text{imp}} \vec{s}(\vec{r}) \rangle d^D r = -\frac{3}{4}. \quad (14)$$

at $T = 0$. The spin-correlation function is isotrop for a generic system. Substituting the dimensionless variable $x = k_F R / \pi$ and angular integration yields

$$\frac{C_D \pi^D}{k_F^D} \int_0^\infty x^{D-1} \chi_\infty(x) dx = -\frac{3}{4}, \quad (15)$$

where D is the dimension, $C_1 = 2$, $C_2 = 2\pi$ and $C_3 = 4\pi$.

For the linear dispersion $\epsilon(|\vec{k}|) = v_F (|\vec{k}| - k_F)$ the Fermi wave vector in the different dimensions is given by $k_F = \pi/2V_u$ in 1D, $k_F = \sqrt{\pi/V_u}$ in 2D and $k_F = (\pi^2/V_u)^{1/3}$ in 3D. The volume of a unit cell V_u in the Fermi wave vector is canceled by the factor $1/V_u$ in $\vec{s}(x)$ after substituting $\vec{s}_c(\vec{r}) = V_u \vec{s}(\vec{r})$ in the correlation function.

Numerically evaluating the sum-rule (15) using our NRG correlation function, we have confirmed the theoretical value of $-\frac{3}{4}$ with an error less than 2% in 1D. Since $\chi_\infty(R) \propto R^{-(D+1)}$ for $R \rightarrow \infty$, the integral kernel $R^{D+1} \chi_\infty(R)$ is very susceptible to numerical errors in higher dimensions. Therefore, the accuracy decreases with increasing dimensions. For distances $k_F R / \xi_K \gg 1$ a very high number of kept states in the NRG calculation are required to prevent the integral $\int_0^\infty R^{D-1} \chi_\infty(R) dR$ from diverging.

For a ferromagnetic coupling the Hamiltonian approaches the local moment (LM) fixed point with a decoupled impurity spin. Using the same argument as above yields the sum-rule

$$\int \langle \vec{S}_{\text{imp}} \vec{s}(\vec{r}) \rangle d^D r = 0. \quad (16)$$

valid for $J < 0$. Consequently, we expect an oscillatory solution for $\chi_\infty(R)$ with sign changes at all length scales and a decay $R^{-\alpha}$ where $\alpha \geq D$: the spin correlation function will be significantly different in the ferromag-

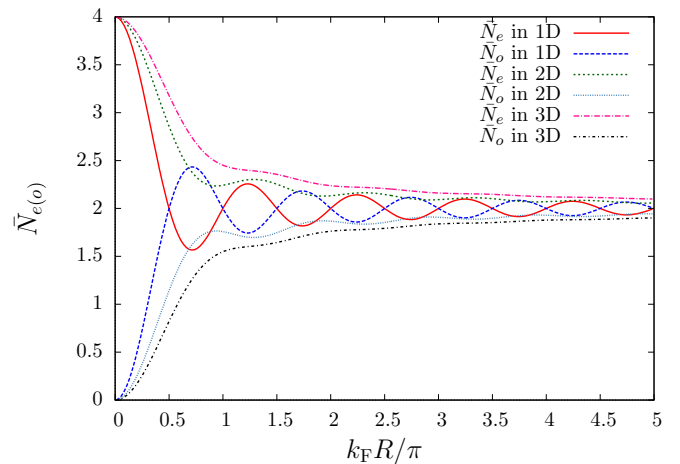


FIG. 1. (Color online) Normalization constants $\bar{N}_{e(o)}$ for different dimensions D vs the dimensionless distance $x = k_F R / \pi$. For $R \rightarrow \infty$ \bar{N}_e is equal to \bar{N}_o .

netic and in the antiferromagnetic regime.

D. Effective densities of states in 1D, 2D and 3D

The spatial correlations depend on the dimensionality of the host. For a given distance R , the dimensionality enters primarily via the dimension of the wave vector \vec{k} in the Eqs. (6) and the energy dispersion $\epsilon_{\vec{k}}$ of the host.

In order to obtain information on generic spectral densities $N_{e(o)}^2(\epsilon)\rho(\epsilon)$ appearing in the Eqs. (8) and (9) we assume a isotropic linear dispersion $\epsilon_{\vec{k}} = v_F (|\vec{k}| - k_F)$, where v_F is the Fermi velocity and k_F the Fermi wave-vector. Inserting the dispersion in equations (6) yields in 1D to

$$N_{e(o)}^2(\epsilon)\rho(\epsilon) = 2\rho_0 \left[1 \pm \cos \left(x\pi \left(1 + \frac{\epsilon}{D} \right) \right) \right] \quad (17)$$

where $\rho_0 = 1/2D$ is the constant density of states and $x = k_F R / \pi$. In higher dimensions we perform the angular integration to obtain for 2D

$$N_{e(o)}^2(\epsilon)\rho(\epsilon) = 2\rho_0 \left[1 \pm J_0 \left(x\pi \left(1 + \frac{\epsilon}{D} \right) \right) \right] \quad (18)$$

with the zeroth Bessel function $J_0(x)$. In 3D, the effective densities of states [31, 32] reads

$$N_{e(o)}^2(\epsilon)\rho(\epsilon) = 2\rho_0 \left[1 \pm \frac{\sin \left(x\pi \left(1 + \frac{\epsilon}{D} \right) \right)}{x\pi \left(1 + \frac{\epsilon}{D} \right)} \right]. \quad (19)$$

Note that in 2D and 3D $\rho(\epsilon)$ is not constant for a linear dispersion, and $\rho(\epsilon) = \rho_0 = 1/2D$ is a simplification.

The normalization constants $\bar{N}_{e(o)}$ reveal important information on the admixture of even and odd bands for a given distance R . They are shown as function of the dimensionless distance $x = k_F R / \pi$ for different dimensions

$\rho_0 J$	T_K/D	$k_F \xi_K$
0.05	$1 \cdot 10^{-10}$	$1 \cdot 10^{10}$
0.075	$1.7 \cdot 10^{-7}$	$5.88 \cdot 10^6$
0.1	$7.5 \cdot 10^{-6}$	$1.33 \cdot 10^5$
0.15	$3.9 \cdot 10^{-4}$	2564.10
0.3	0.0204	49.02
0.5	0.0749	13.35
0.6	0.115	8.69
0.7	0.2103	4.76

TABLE I. The Kondo temperature T_K and length scale ξ_K for different Kondo couplings. The Kondo temperatures have been obtained from the NRG level flow - see text.

D in Fig. 1. Clearly, $\bar{N}_o(x=0) = 0$ in any dimension: The odd band decouples from the problem, and the standard Kondo model is recovered which allows to calculate local ($R=0$) expectation values within the standard single band NRG [35].

With increasing R , the oscillations of the even and odd density of states $\rho_{e(o)}$ decay as $\propto R^{(1-D)/2}$. For large distances, the even and odd bands become equal and the normalization constants approach the same value. For 1D, strong oscillations are observed for short distances which are suppressed in higher dimensions. Apparently the R dependency will be more pronounced in lower dimensions and the correlation function will decay with the different power law than in higher dimensions.

III. EQUILIBRIUM PHYSICS: SPATIAL CORRELATION

A. Kondo regime: Short distance vs large distance properties

There are two characteristic length scales in the problem: $1/k_F$ defined by the metallic host, governing the power-law decay of $\chi_\infty(R)$ and its RKKY oscillations, and the Kondo length scale ξ_K , sometimes referred to as size of the Kondo screening cloud [23–26, 28]. Since ξ_K increases exponentially with decreasing J , we use different J to present data for the two different regimes $R < \xi_K$ and $\xi_K < R$. The results for $\chi_\infty(R)$ for these two different regimes are shown in Fig. 2.

In our calculations, the Kondo temperature T_K has been defined from the NRG level flow: T_K is the energy scale at which the first excitation reaches 80 % of its fixed point value. The Kondo temperature T_K and length scale ξ_K for different Kondo couplings are stated in Tab. I. All correlation functions have been obtained for $T/T_K \rightarrow 0$. The sum-rule (15) of $\chi_\infty(R)$ is numerically fulfilled up to typically 2% error in 1D.

In contrast to the original work by Borda [27], we observe ferromagnetic and anti-ferromagnetic correlations for short distances in accordance with predictions [23–

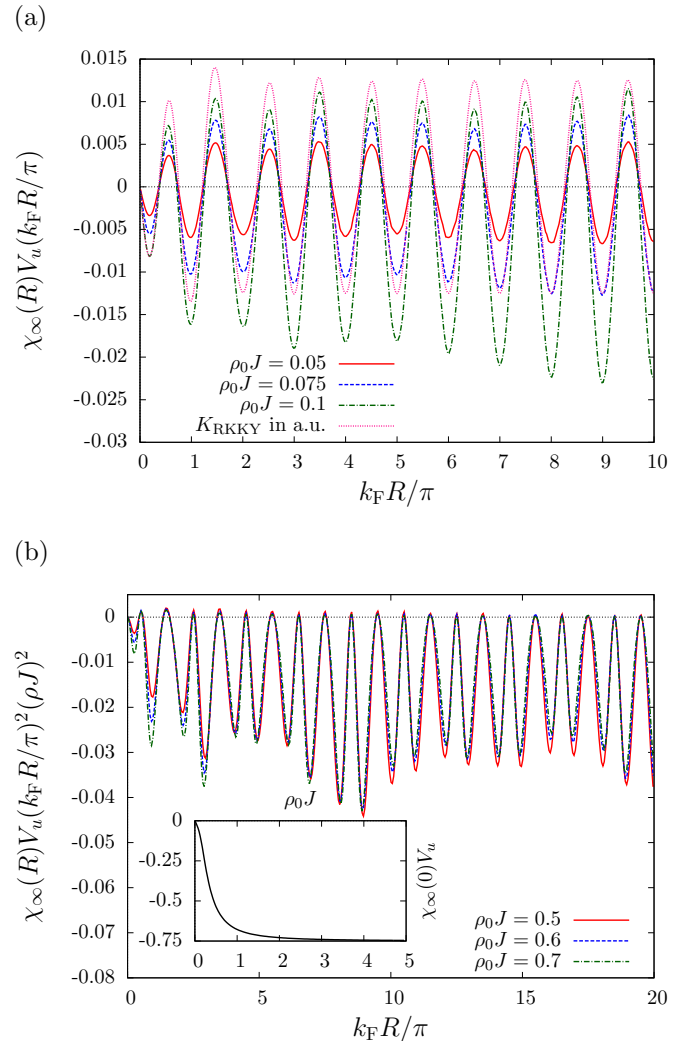


FIG. 2. (Color online) The spin-correlation function (a) $R\chi_\infty(R) = R\langle\vec{S}_{\text{imp}}\vec{s}(\vec{r})\rangle$ as a function of the dimensionless distance $x = k_F R/\pi$ in 1D for small Kondo couplings $\rho_0 J = 0.05, 0.075, 0.1$ and $k_F R/\xi_K \ll 1$. We added RKKY-interaction between the impurity spin and a probe spin in distance R for comparison. (b) $R^2\chi_\infty(R)$ as a function of the dimensionless distance x in 1D for larger Kondo couplings $\rho_0 J = 0.5, 0.6, 0.7$. The inset shows the value of the correlation function at the origin $\chi_\infty(0)$ vs ρJ . For large J the value $-3/4$ is reached.

26, 28] by Affleck and his collaborators as presented in Fig. 2(a). For distances $R \ll \xi_K$ the impurity is still unscreened and impurity spin behaves more like a free spin. We have plotted the rescaled correlation function $R\chi_\infty(R)$ to reveal the $1/R$ decay at short distances in 1D [27] stemming from the analytical form of the RKKY-interaction.

We have also added the RKKY-interaction K_{RKKY} between the impurity spin and a fictitious probe impurity spin at distance R obtained in second order perturbation theory for comparison – details of the calculations can be found in Appendix A. The oscillating part of $\chi_\infty(R)$,

and the positions of the minima and maxima nicely agree with the RKKY-interaction $\propto \cos(2k_F R)$. For multiple integers $x = k_F R/\pi = n$ the correlation function has minima and for odd multiple $x = n + 1/2$ a maxima is found.

In order to access larger distances $R \gg \xi_K$, we increase $\rho_0 J$. The rescaled spin correlation function $R^2 \chi_\infty(R)$ depicted in Fig. 2(b) clearly reveals the power-law decay of the envelop function at distances $R/\xi_K \gg 1$ as $1/R^2$. Furthermore, we only find antiferromagnetic correlations for $R/\xi_K \gg 1$, and $\chi_\infty(R)$ remains negative at all distances. In this regime, the maxima have the value $\chi_\infty(R) = 0$ as noted earlier [23–26, 28]: The impurity spin is screened by the conduction band electrons and the envelope of $\chi_\infty(R)$ has to decrease faster.

We observe this crossover from a $1/R$ to a $1/R^2$ decay at around $R \approx \xi_K$. We also find universal behavior for the envelope of $\chi_\infty(R)$ for distances $k_F R/\pi > 1$ and can reproduce Fig. 3 of Ref. [27] (not shown here.)

Since we have plotted $R^2 \chi_\infty(R)$ which vanishes for $R = 0$, the information of $\chi_\infty(0)$ is not included in the main panels of Fig. 2. Therefore, we have added the $\rho_0 J$ dependency of the local spin-correlation function $\chi_\infty(R = 0)$ as inset to Fig. 2(b). $\chi_\infty(0) < 0$, as expected for a local antiferromagnetic coupling, and the strong coupling value of $-3/4$ is approached for large J : almost the whole contribution to the sum-rule (15) is located in the first antiferromagnetic peak at $R = 0$, and $\chi_\infty(R)$ has to decay very rapidly with increasing R .

In Fig. 3 the short distance behavior of $\chi_\infty(R)$ in 2D is shown. As for 1D case the oscillating part and the positions of the minima and maxima of $\chi_\infty(R)$ and the 2D RKKY-interaction nicely agree. In contrast to 1D the RKKY-interaction acquires a more complex mathematical structure even for a simplified linear dispersion replacing the simple $\cos(2k_F R)$ oscillations in 1D. Therefore, modification to the $\cos(2k_F R)$ behavior must be taken into account when analyzing experimental data.

B. Ferromagnetic couplings $J < 0$ in 1D

Up until now, we have focused only on antiferromagnetic Kondo coupling causing the Kondo-singlet formation described by the strong-coupling (SC) fixed point for $T \rightarrow 0$. We extend our discussion of the equilibrium correlation function to the ferromagnetic regime characterized by the local-moment (LM) fixed point and a twofold degenerate ground state. As pointed out above, the sum-rule for $\chi_\infty(\vec{r})$ predicts that the spatial integral of the correlation function vanishes. For a ferromagnetic coupling $\xi_K \rightarrow \infty$, and the correlation function is also oscillating as $\cos(2k_F R)$ and decaying as $1/R$ for all distances in 1D.

Exemplifying our findings, we depicted $R\chi_\infty(R)$ for two different Kondo coupling, $\rho_0 J = -0.1$ and $\rho_0 J = -0.5$, in Fig. 4. We numerically checked the sum rule and found deviations from zero by less than 1% in 1D. The

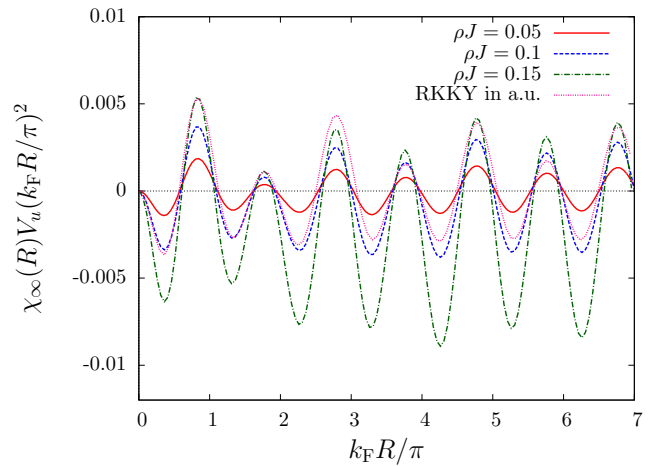


FIG. 3. (Color online) The spin-correlation function $R^2 \chi_\infty(R)$ as a function of the dimensionless distance $x = k_F R/\pi$ in 2D. In higher dimensions the envelope of the RKKY and $\chi_\infty(R)$ has a more complicated structure. Every second maximum has a lower amplitude. NRG parameters: $\Lambda = 5$, $N_s = 3000$

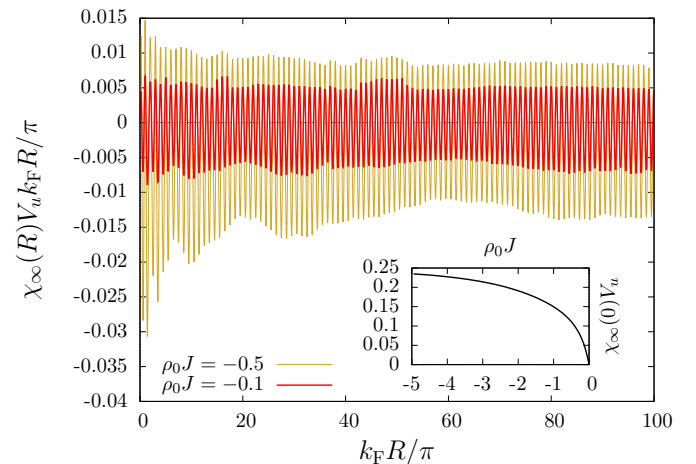


FIG. 4. (Color online) The spin-correlation function $R\chi_\infty(R)$ as a function of the dimensionless distance $x = k_F R/\pi$ in 1D for two different ferromagnetic Kondo couplings $\rho_0 J = -0.1$ and $\rho_0 J = -0.5$ for $T \rightarrow 0$. The inset shows $\chi_\infty(0)$ vs $\rho_0 J$. For large ferromagnetic couplings 0.25 is reached. NRG parameters: $\Lambda = 3$, $N_s = 1400$

RKKY oscillations and $1/R$ decay of the envelop function are clearly visible up very larger distances $k_F R/\pi = 100$.

In the ferromagnetic regime, the local spin-correlation function $\chi_\infty(0)$ must be positive and approaches its upper limit of $\chi_\infty(0) \rightarrow 1/4$ for $J \rightarrow -\infty$ as shown in the inset of Fig. 4. In order to fulfil the sum-rule $\chi_\infty(R)$ does not oscillate symmetrically around the x-axis: $\chi_\infty(R)$ must be slightly shifted to antiferromagnetic correlations to compensate the ferromagnetic peak at $R = 0$.

IV. NON-EQUILIBRIUM DYNAMICS

A. Extension of the NRG to non-equilibrium: the TD-NRG

The TD-NRG has been designed [17] to track the real-time dynamics of quantum-impurity systems following an abrupt quantum quench such as considered here: at $t = 0$ we switch on the Kondo coupling J between the prior decoupled impurity spin and the metallic host.

Initially, the entire system is characterized by the density operator of the free electron gas

$$\hat{\rho}_0 = \frac{e^{-\beta H_0}}{\text{Tr}[e^{-\beta H_0}]}, \quad (20)$$

at time $t = 0$ when the Kondo interaction H_K is suddenly switched on: $H = H_0 + H_K$. The density operator evolves thereafter in time according to

$$\hat{\rho}(t > 0) = e^{-itH} \hat{\rho}_0 e^{itH}. \quad (21)$$

Our objective is to use the NRG to compute the time-dependent expectation value $O(t)$ of a general local operator \hat{O} . As shown in Refs. [17], the result can be written in the form

$$\langle \hat{O} \rangle(t) = \sum_m \sum_{r,s}^{\text{trun}} e^{it(E_r^m - E_s^m)} O_{r,s}^m \rho_{s,r}^{\text{red}}(m), \quad (22)$$

where E_r^m and E_s^m are the dimension-full NRG eigenenergies of the perturbed Hamiltonian at iteration $m \leq N$, $O_{r,s}^m$ is the matrix representation of \hat{O} at that iteration, and $\rho_{s,r}^{\text{red}}(m)$ is the reduced density matrix defined as

$$\rho_{s,r}^{\text{red}}(m) = \sum_e \langle s, e; m | \hat{\rho}_0 | r, e; m \rangle. \quad (23)$$

The restricted sum over r and s in (22) requires that at least one of these states is discarded at iteration m . The NRG chain length N implicitly defines the temperature entering Eq. (20): $T_N \propto \Lambda^{-N/2}$, where $\Lambda > 1$ is the Wilson discretization parameter.

The derivation of Eq. (22) is based on the two observations. (i) It has been shown [17] that the set of all discarded states in the NRG procedure forms a complete basis set of many-body Fock space which are approximate eigenstates of the Hamiltonian. (ii) The general local operator \hat{O} is diagonal in the environment degrees of freedom (DOF) such that the trace over these DOF can be performed analytically yielding $\rho_{s,r}^{\text{red}}(m)$. This approach has been extended to steady state currents at finite bias [36–38]. The only error of the method stems from the representation of the bath continuum H_0 by a finite-size Wilson chain[11] and are essentially well understood [39, 40].

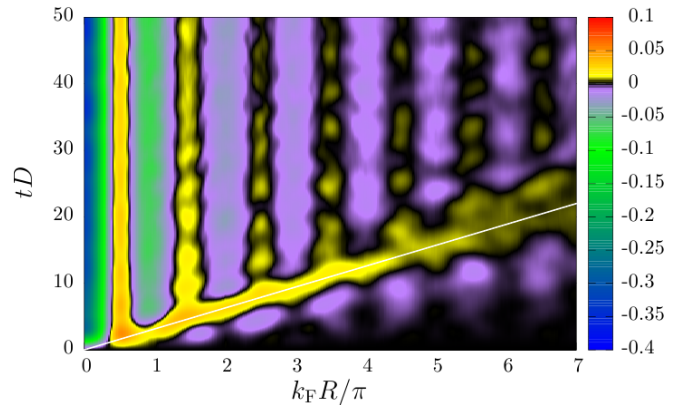


FIG. 5. (color online) The 1D time and spatial dependent spin-correlation function $\chi(R, t)$ vs $x = k_F R / \pi$ and $\tau = tD$ for $\rho_0 J = 0.3$ as color contour plot. Its color map is depicted on the right site. The correlation propagates with v_F which is added as white line as guide to the eye. NRG parameters: $\Lambda = 3$, $N_s = 1200$, $N_z = 4$.

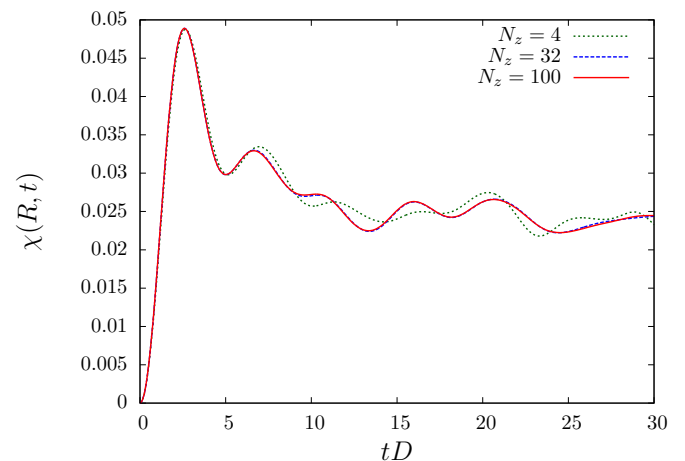


FIG. 6. (color online) Time dependent correlation function $\chi(R, t)$ for a fixed distance $k_F R / \pi = 0.51$ vs time for different number of z -averages N_z and a fixed $\rho_0 J = 0.3$. NRG Parameters: $\Lambda = 3$, $N_s = 1600$.

B. Time-dependent spatial correlation function in the Kondo regime

After discussing the equilibrium correlation function in Sec. III, we present our results for the full time-dependent correlation function $\chi(\vec{r}, t)$. The NRG fixed point differs for different signs of the Kondo coupling: for $J > 0$ the SC fixed point [11] is reached while for $J < 0$ the system approaches the LM fixed point. Therefore, we present data for both regimes and begin with the antiferromagnetic Kondo coupling.

$\chi(R, t)$ is depicted as function of the dimensionless distance $x = k_F R / \pi$ and the dimensionless time $\tau = tD$ for a moderate Kondo coupling $\rho_0 J = 0.3$ as a color contour plot for 1D in Fig. 5. Each distance R requires a single

TD-NRG run. Therefore, we have restricted ourselves to $N_z = 4$ z-values for the z-averaging [17, 41] for the $N_R = 350$ different values of R included in Fig. 5 and only kept a moderate number of NRG states.

The development of the ferromagnetic correlation maximum at $x = 1/2$ is clearly visible already after very short times corresponding to $\chi_\infty(R)$ depicted in Fig. 2(a). For $t \rightarrow \infty$, the equilibrium Friedel oscillations as discussed above are recovered: the correlation function has minima for $x = n$, and maxima are found for odd multiple $x = n + 1/2$. For larger distances and times the ferromagnetic correlations are suppressed in favor of purely antiferromagnetic correlations as expected from the equilibrium correlation function.

After the ferromagnetic correlation maximum has passed, $\chi(R, t)$ exhibits some weak oscillations in time for $R = \text{const}$. In order to discriminate between finite size oscillations caused by the bath discretisation [17, 39, 40] and the real non-equilibrium dynamics of the continuum, the time evolution of $\chi(R = 0.51\pi/k_F, t)$ is shown for different number of z-averages N_z in Fig. 6. Since the short-time oscillations clearly converge with increasing N_z , they contain relevant real-time dynamics which will be analysed in more detail in the next section below. In the long-time limit, the TD-NRG oscillates around a time average which is independent of N_z and is close to equilibrium correlation function $\chi_\infty(R)$. Those oscillations are partially related to the bath discretisation [17, 39, 40] and are suppressed for increasing number of z-values N_z , decreasing Λ and increasing number of N_s . Therefore, we conclude that thermodynamic equilibrium is reached up to the well understood small discretisation errors [17, 39, 40].

1. *How are the Kondo correlation building up at different distances R with time?*

Clearly visible is the propagation of ferromagnetic correlations away from the impurity with a constant velocity given by the Fermi-velocity of the metallic host. At the impurity site, an antiferromagnetic spin-spin correlation develops rather rapidly. Since the total spin is conserved in the system, a ferromagnetic correlation-wave propagates spherically away from the impurity spin. The added white line $R = v_F t$ serves as guide to the eye in Fig. 5 to illustrate this point. This line represents the analog to a light-cone in electrodynamics.

Inside the light-cone, the equilibrium correlation function is reached rather fast. To exemplify this, we plot $\chi(R, t)$ as function of relative time $t' = t - R/v_F$ for four different distances R in Fig. 7(a). Negative t' corresponds to the response outside the light-cone, while for $t' > 0$ the spin correlation function $\chi(R, t)$ inside the light cone is depicted.

At the origin of the impurity ($R = 0$), a antiferromagnetic correlation develops [42] on the time scale $1/\sqrt{J}$: the short time dynamics is linear in the Kondo coupling

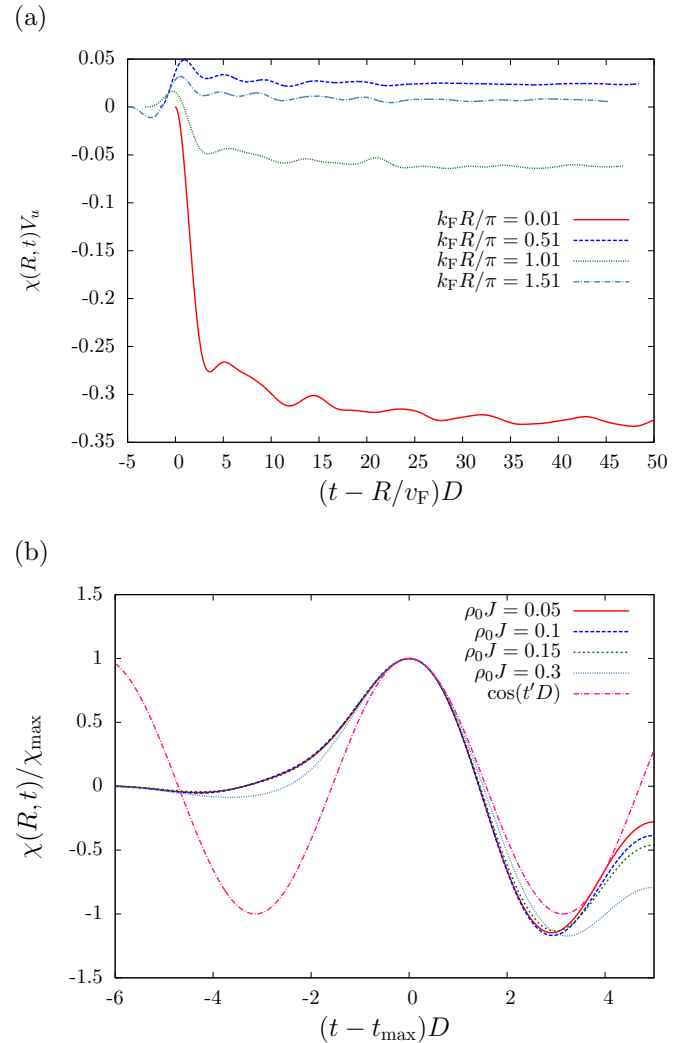


FIG. 7. (color online) (a) Time dependent correlation function $\chi(R, t)$ vs $t' = t - R/v_F$ for four different distances $k_F R = 0, 0.51, 1.01, 1.51$ for $\rho_0 J = 0.3$ in 1D. (b) Rescaled time dependent correlation function $\chi(R, t)/\chi_{\max}$ vs $t - t_{\max}$ for $k_F R/\pi = 2.01$ and four different couplings $\rho_0 J = 0.05, 0.1, 0.15, 0.3$. t_{\max} is the position and χ_{\max} is the amplitude of the ferromagnetic peak. NRG Parameters: $\Lambda = 3, N_s = 1200, N_z = 32$.

and proportional to t^2 as will be discussed in greater detail below.

At $t' = 0$ and finite distance $R > 0$, a significant ferromagnetic correlation-wave peak is observed which decays rather rapidly. Its position corresponds to the yellow (color-online) light-cone shown in Fig. 5. In order to shed some light into the nature of this rapid decay, we present the ratio $\chi(R, t)/\chi_{\max}$ vs $(t - t_{\max})D$ for a constant distance $k_F R/\pi = 2.01$ and different couplings $\rho_0 J$ in Fig. 7(b). χ_{\max} has been defined as $\chi_{\max} = \chi(R, t_{\max})$, and t_{\max} is the numerical position of the ferromagnetic peak. Note that t_{\max} slightly differs from bare light-cone time scale R/v_F and is shifted to larger times with increasing $\rho_0 J$ (not shown.) This increasing shift can

be analytically understood, and we will give the detailed explanation in Sec. IV C below. After dividing out the amplitude χ_{\max} of the maximum, the decay surprisingly shows a universal behavior and the time scale is simply given by $1/D$. A comparison of the oscillation with $\cos(t'D)$ (pink dash-dotted line) shows a remarkable agreement for small times $0 < t'D < 1$. This indicates that the functional form of $\chi(R, t)$ for fixed R consists of a damped oscillatory $\cos(t'D)$ term whose maximum is reached when the ferromagnetic correlation wave reaches the distances R at the time $t_{\max} > R/v_F$. For larger times t' , $\chi(R = 2.01\pi/K_F)$ has to approach a finite antiferromagnetic value. Therefore, the oscillations in the TD-NRG are not centered around the origin but shifted to negative values as can be seen in Fig. 7(b) by comparing with the undamped $\cos(t'D)$ curve.

Most striking, however, is the building up of correlations for $t' < 0$ outside of the light-cone. These correlations are antiferromagnetic and show no exponential decay. These correlations appear shortly before the light cone. They reach their largest modulus for odd multiple $k_F r/\pi = n + 1/2$ and decay with a power law as tD goes to zero. In Sec. IV D below, we will provide a detailed analysis of their origin and present an analytical calculation in J which agrees remarkably well with the observed TD-NRG results.

Such a building up of correlations outside of the light-cone has recently been reported in a perturbative calculation [22] neglecting, however, the $2k_F$ oscillations. Here, we present results for a full non-perturbative calculation which includes the Friedel oscillations containing the RKKY mediated effective spin-spin interaction.

The different behavior for short and long distances is illustrated in Fig. 8. The upper panel shows results for short distances $r/\xi_K \ll 1$. We observe the distinctive ferromagnetic correlation which propagates with the Fermi velocity through the conduction band. Inside the light cone we find oscillations between ferromagnetic and antiferromagnetic correlations. In the lower panel the behavior for longer distances is depicted. We find that the ferromagnetic propagation vanishes at around $k_F R \approx \xi_K$. At these distances, we only observe oscillations between zero and antiferromagnetic correlations inside the light cone. For both cases the long-time behavior agrees remarkably well with the NRG equilibrium calculations.

C. Perturbation theory

Surprisingly, we found in our TD-NRG results the building up of spin-correlations outside of the light-cone which do not decay exponentially. In order to rule out TD-NRG artefacts and shed some light into its origin, we perturbatively calculate $\langle \vec{S}_{\text{imp}} \vec{s}(r) \rangle(t)$ up to second order in J .

Since only H_0 enters the initial density operator, we transform all operators into the interaction picture and, after integrating the von Neumann equation, we obtain

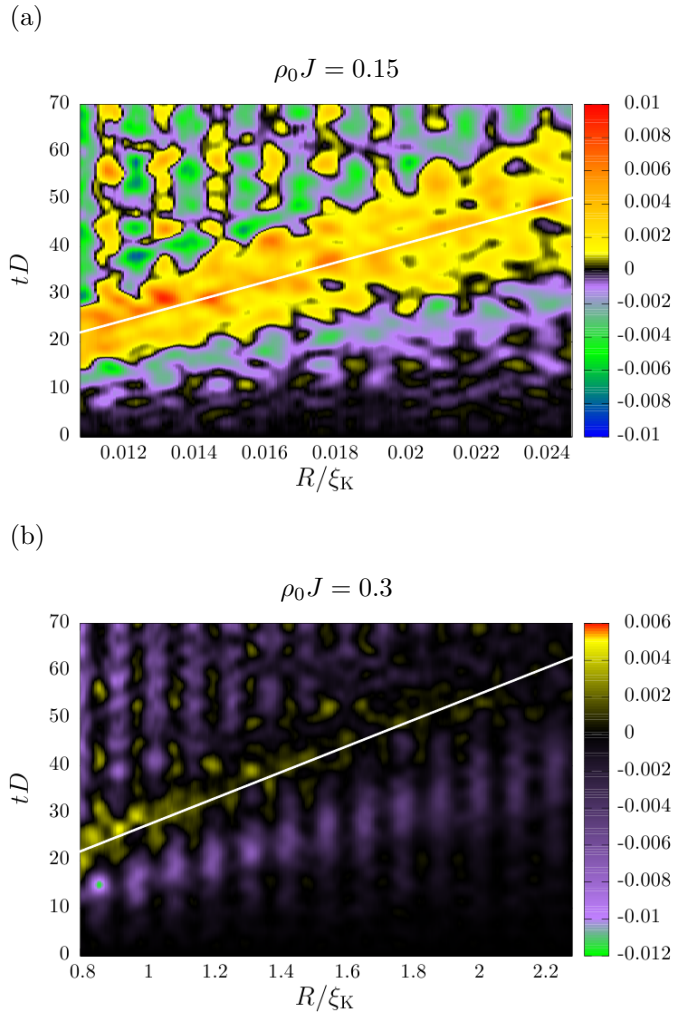


FIG. 8. (Color online) The time dependent correlation $\langle \vec{S}_{\text{imp}} \vec{s}(R) \rangle(t)$ for different distances as color contour plot. Its color map is depicted on the right side. (a) The oscillation between ferromagnetic and antiferromagnetic correlations for long times is only observed for short distances $R/\xi_K \ll 1$. (b) For long times oscillations only between zero and antiferromagnetic correlations are observed. The ferromagnetic propagation vanishes at around $R/\xi_K \approx 1$. Both long-time behavior are in agreement with the NRG equilibrium results.

for the density operator

$$\rho^I(t) \approx \rho_0 + i \int_0^t [\rho_0, H_K^I(t_1)] dt_1 - \int_0^t \int_0^{t_1} [[\rho_0, H_K^I(t_2)] H_K^I(t_1)] dt_2 dt_1 \quad (24)$$

which is exact in second order in the Kondo coupling J . The superscript I labels the operators in interaction picture $A^I(t) = e^{iH_0 t} A e^{-iH_0 t}$, and the boundary condition is given by $\rho_0 = \rho^I(t=0)$. We use this $\rho^I(t)$ to calculate the spin-spin correlation function

$$\chi(\vec{r}, t) = \text{Tr} \left[\rho^I(t) \vec{S}_{\text{imp}} \vec{s}^I(\vec{r}, t) \right] \quad (25)$$

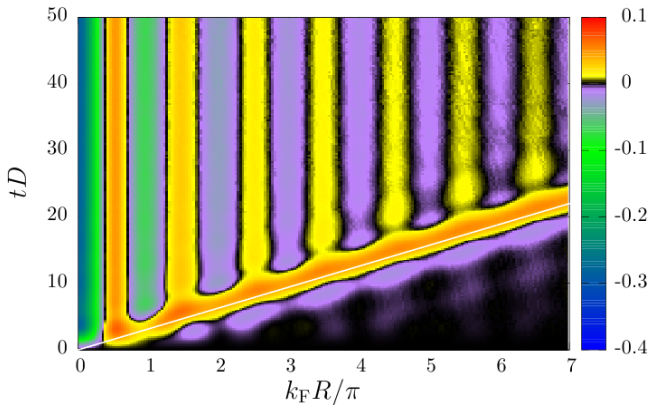


FIG. 9. (Color online) The analytical $\chi(R, t)$ evaluated numerically for $\rho_0 J = 0.3$ up to second order in J as color contour plot. Its color map is depicted on the right site. The light-cone $R = v_F t$ has been added as a white line.

where only expectation values with respect to the initial density operator ρ_0 enter. The occurring commutators are cumbersome but can be evaluated analytically - for details see appendix B. We note that the contribution in linear order in J does not vanish for a perturbation $H_K = J \vec{S}_{\text{imp}} \vec{s}(0)$. Although the time integrals can be performed analytically, the multiple momenta integrations of the free conduction electron states must be performed numerically.

The sum of the first and second order contributions to $\chi(R, t)$ are shown in Fig. 9 up to relatively large times. This perturbatively calculated $\chi(R, t)$ turns out to be well behaved and does not contain secular terms. Clearly, the Kondo physics is not included in such an approach remaining only valid for $r/\xi_K \ll 1$ and $tT_K \ll 1$. Therefore, we expect deviations at large distances and times from the NRG results.

Nevertheless, the NRG result depicted in Fig. 5 and the perturbation theory result qualitatively agrees very well. As in the TD-NRG, ferromagnetic correlations propagate spherically away from the impurity with Fermi velocity (white line as guide to the eye) in the perturbative solution. For long times an equilibrium is reached: we recover the distance dependent Friedel oscillations which are known from the RKKY interaction. We also find the same antiferromagnetic correlations outside the light cone as in the NRG results. Again, their maxima are located at odd multiple of $x = k_F R / \pi = n + 1/2$ at the same positions as predicted in the TD-NRG calculations.

To the leading order in the Kondo coupling $\rho_0 J$, the ferromagnetic wave in the correlation function propagates on the the light-cone line $R = v_F t$. Note, however, that the peak position of the analytical $\chi(R, t)$ plotted in Fig. 9 is slightly shifted to later times than defined by the light-cone line. This shift coincides with the one observed in the TD-NRG results shown in the Figs. 5 and 7. With our analytical analysis at hand, we can provide a detailed understanding of this effect. The first order contribution

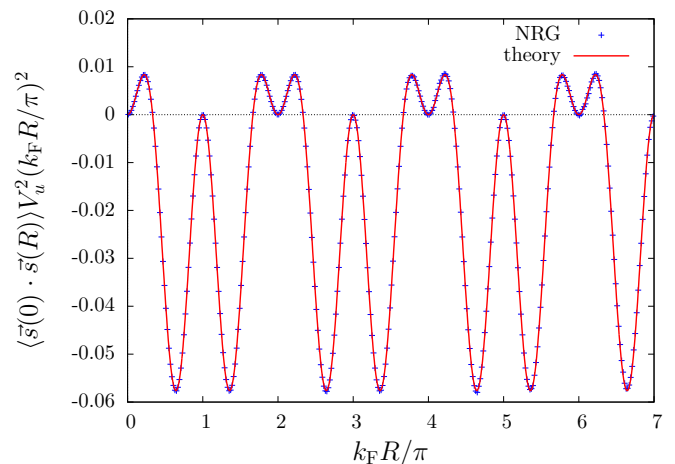


FIG. 10. (Color online) The intrinsic spin-spin correlations of the Fermi sea between the spin densities $\vec{s}(0)$ and $\vec{s}(r)$ in 1D. Via the mapping to the even and odd conduction bands we are able to measure bath properties at distance R and get a perfect agreement between theory and NRG results. NRG parameters: $\Lambda = 3$, $N_s = 1200$.

given by Eq. (B6) yields a peak of ferromagnetic correlations positioned exactly on light-cone line. However, the maximum of the second order contribution (B7) is shifted to slightly larger times. Adding both contributions generates a J -dependent line for the ferromagnetic peak position away from the light-cone line: the larger J , the later the ferromagnetic maximum occurs due to increasing importance of the second order contribution.

While these spatial oscillations are implicitly encoded in the effective even and odd density of states in the NRG calculation, they are explicitly generated by the momenta integration in the perturbative approach. This confirms our TD-NRG results and provides a better understanding of the numerical data.

Comparing Fig. 5 and Fig. 9 in more detail illustrates the shortcomings of the perturbative approach which remains only valid for $R/\xi_K \ll 1$. As discussed in Sec. III above, the decay of the envelope function crosses over from a $1/R$ to an $1/R^2$ behavior due to the Kondo screening of the local moment for $R/\xi_K > 1$. Since the perturbative approach is unable to access the Kondo-singlet formation the perturbative solution depicted in Fig. 9 decays as $1/R$ at all distances and also remains oscillating between ferromagnetic and antiferromagnetic correlations while the TD-NRG correctly predicts only antiferromagnetic correlations inside the light-cone once R exceeds the Kondo length scale ξ_K .

D. Intrinsic correlations of the Fermi sea

Since the perturbative results agree remarkably well with the TD-NRG data for short distances, the analytical approach can be used to gain an explicitly under-

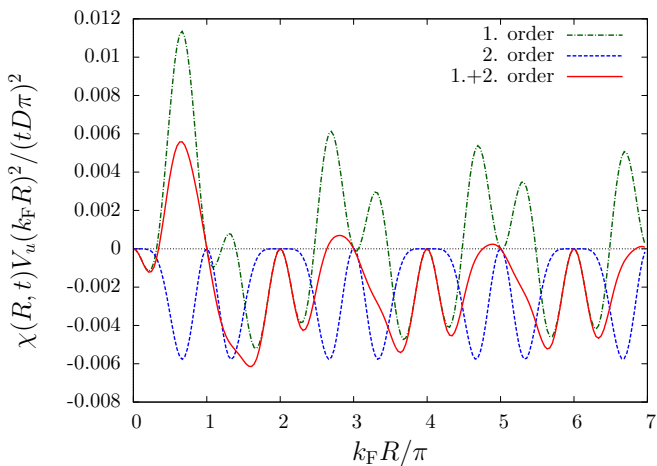


FIG. 11. (Color online) First and second order of $\chi(R, t)$ for small times t and $\rho_0 J = 0.3$ in 1D. Even for short times we observe correlations for large distances. A comparison with a) shows that the positions of these correlations coincide with the positions of the intrinsic correlations of the Fermi sea. So the correlations outside the light cone originate from these intrinsic correlations.

standing of the correlations outside of the light-cone. It has been proposed [22] that these correlations originate from the intrinsic spin-spin correlations in the Fermi sea $\langle \vec{s}(0)\vec{s}(\vec{r}) \rangle$ already present prior to the coupling of the impurity. Once the impurity is coupled to the local conduction electron spin density at time $t = 0$, we instantaneously probe these intrinsic entanglements of the Fermi sea between the local spin density and the spin density at a large distance R .

For $J = 0$, $\langle \vec{s}(0)\vec{s}(R) \rangle$ can be calculated analytically and is given by

$$\langle \vec{s}(0)\vec{s}(R) \rangle = \frac{3 \sin(k_F R) \sin(\frac{k_F R}{2}) \cos(\frac{3}{2}k_F R)}{4V_u^2(k_F R)^2} \quad (26)$$

in 1D. This exact result coincides with the NRG data obtained by setting $J = 0$ in an equilibrium NRG calculation as shown in Fig. 10. This excellent agreement between the analytical and the NRG approach serves as further evidence for the numerical accuracy of mapping Eqs. (7-9) to the two discretised and properly normalised Wilson chains for even and odd parity conduction bands.

In order to connect the intrinsic spin-entanglement of the decoupled Fermi sea with the observed antiferromagnetic correlations outside of the light cone, we expand the perturbative calculated $\chi(R, t)$ for small times $0 \leq tD \ll 1$ and perform the momentum integrations analytically, separately for the first and the second order contribution.

The leading order terms in time are proportional to $\propto (tD)^2$ and decays as $1/R^2$. Remind the difference between the $1/R^2$ decay outside of the light-cone for the short-times dynamics and the well understood $1/R$ decay inside the light-cone when the equilibrium reached.

Therefore, we have plotted the perturbative results in 1D as $\chi(R, t)(R/(tD))^2$ in Fig. 11 to eliminate the time dependency and compensate for the leading spatial decay of the envelop function. The first-order contribution (green online) is shown as dashed-dotted line, the second-order contribution (blue online) is depicted as dashed line, and the sum of both (red online) is added as solid line for $\rho_0 J = 0.3$ in Fig. 11.

Since second-order contribution to $\chi(0, t)$ remains always zero in a short-time expansion, the time evolution of the antiferromagnetic correlation at $R = 0$ is dominated by the first-order term being proportional to $\propto Jt^2$. Therefore, the time scale for the initial fast buildup of the local antiferromagnetic correlation is given by $1/\sqrt{J}$ confirming the TD-NRG short-time dynamics for $k_F R/\pi = 0.01$ as depicted in Fig. 7(a).

The largest contribution for short times stems from the ferromagnetic peak around $k_F R/\pi = 0.5$. However, correlations are visible at all length scales which develop quadratically in time. The positions of the maxima and minima agree remarkable with those of the intrinsic correlation function $\langle \vec{s}(0)\vec{s}(R) \rangle$ of the Fermi sea depicted in Fig. 10 and both decay with $1/R^2$.

Since first-order contribution is sensitive to the sign of J , its maxima contribute with the equal sign as $\langle \vec{s}(0)\vec{s}(R) \rangle$ for ferromagnetic J and opposite sign for an antiferromagnetic coupling. The second-order term only adds negative (antiferromagnetic) contributions to $\chi(R, t)$. The location of its negative peaks coincide with the antiferromagnetic peak location of the spin-spin correlation function $\langle \vec{s}(0)\vec{s}(\vec{r}) \rangle$ of the decoupled Fermi sea depicted in Fig. 10. The sum of both orders contain only small ferromagnetic correlations for larger distances $k_F R/\pi > 1$ for $\rho_0 J = 0.3$. The larger the coupling J is the smaller these ferromagnetic correlations are due to the increasing dominance of the second order term.

We can conclude from this detailed analytical analysis that the antiferromagnetic correlation directly in front of the light cone results from the antiferromagnetic peak in the intrinsic correlations from the Fermi sea at around $k_F R \approx 1.6\pi$. This peak also propagates through the conduction band with the Fermi velocity. Because the intrinsic correlations decay with $1/(k_F R)^2$ the propagation of the antiferromagnetic peaks for larger distances are not visible.

E. Local moment regime: ferromagnetic coupling: $J < 0$

Now we extend the discussion to ferromagnetic Kondo couplings. In this regime, the LM fixed point is stable, and the ground state is two-fold degenerate in the absence of an external magnetic field. In the RG process, the Kondo coupling is renormalised to zero. Nevertheless, the spatial spin-correlation function $\chi_\infty(R)$ remains finite for $T \rightarrow 0$ as discussed in Sec. III B.

The results for time-dependent spin-correlation func-

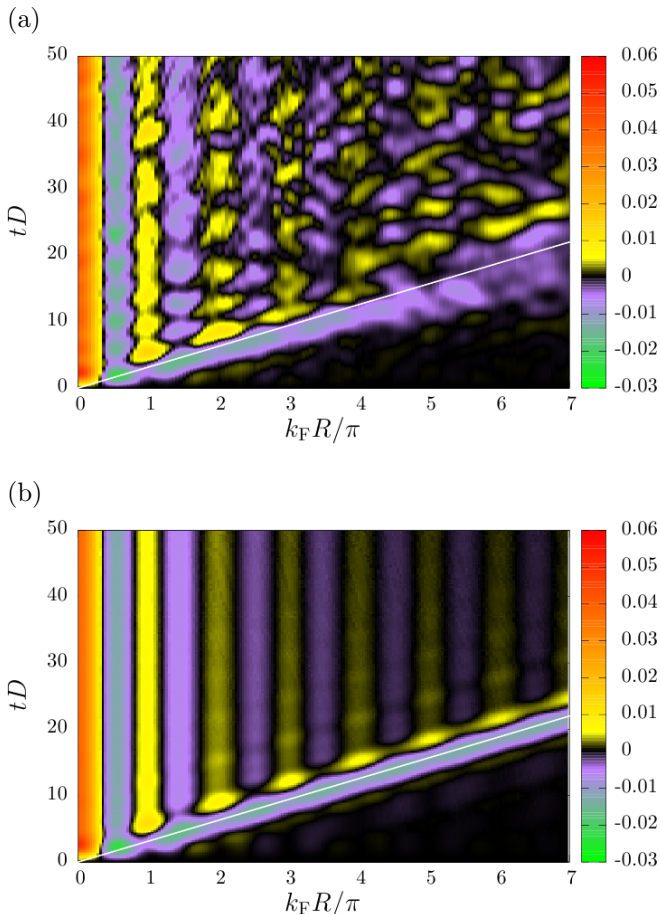


FIG. 12. (Color online) (a) The time dependent spin correlation function $\chi(R, t)$ vs $x = k_F R / \pi$ and $\tau = tD$ for a ferromagnetic Kondo coupling $\rho_0 J = -0.1$ in 1D as color contour plot. Its color map is depicted on the right site. (b) The analytical spin correlation function $\chi(R, t)$ for the same parameter calculated in second order perturbation theory in $\rho_0 J$. NRG parameters: $\Lambda = 3$, $N_s = 1400$, $N_z = 4$.

tion $\chi(R, t)$ are shown as color contour plot in Fig. 12. Figure 12(a) depicts the TD-NRG calculation while the analytical result obtained up to second-order perturbation theory is added as panel (b) for the same parameters. Since the first order contribution is sign sensitive, the analytical response function differs significantly from the antiferromagnetic regime displayed in Fig. 9.

As in the Kondo regime, the analytical and the TD-NRG results agree qualitatively very well. The Friedel oscillations with the frequency $2k_F$ are clearly visible inside the light-cone. Note the phase shift compared to the Kondo regime: now the ferromagnetic correlations are observed at $x = n$ and the antiferromagnetic correlations at half integer values of x .

Since a ferromagnetic correlation is building up at the impurity spin position on a very short time scale $\propto 1/\sqrt{J}$, and the total spin of the system is conserved, an antiferromagnetic correlation wave spherically propagates away from the origin traveling with the Fermi-velocity v_F

(again we have added a white line $R = v_F t$ as guide to the eye to both panels). For ferromagnetic couplings the peak position of the propagation is slightly shifted to earlier times $t_{\max} < R/v_F$, due to the sign change of the first order contribution. The response outside the light-cone is stronger suppressed compared to the Kondo-regime. Again, we can trace the origin to the intrinsic entanglement of the Fermi sea by consulting Figs. 10 and 11 as well as the discussion above.

V. DISCUSSION AND OUTLOOK

We presented a comprehensive study of the spatial and temporal propagation of Kondo-correlations for antiferromagnetic and ferromagnetic Kondo couplings using the TD-NRG.

Our approach is based on a careful construction of two Wilson chains obtained from the two distance dependent even and odd parity bands. The full energy dependency and the correct normalisation of the bands are required for accurate results. We have benchmarked our mapping by (i) calculating the intrinsic spatial dependency of spin-spin correlation of the Fermi sea which coincides with the exact analytical calculation for the full continuum, and (ii) checking the sum-rule of the equilibrium spin correlation function for ferromagnetic and antiferromagnetic couplings. Our numerical data fulfil the sum-rule with an error of 1% in 1D which provided a second independent check of the distance dependent NRG mapping.

The light-cone defined by the Fermi-velocity $R = v_F t$ divides parameter space of the spatial and temporal correlation function $\chi(R, t)$ in two segments. Inside the light-cone, the spin correlations develop rather rapidly, and then followed by a much slower decay towards the equilibrium correlation function. The typical decaying Friedel oscillations with a characteristic frequency $2k_F$ are observed in the spatial dependency. In the Kondo regime, the envelope function shows a power-law behavior $1/R$ in equilibrium with ferromagnetic and antiferromagnetic correlations for short distances and crosses over to a $1/R^2$ behavior for distances exceeding the Kondo length scale $R > \xi_K$ in 1D. In this region only antiferromagnetic correlations are found which correspond to a finite negative value of the sum-rule.

For ferromagnetic regime, the inverse length scale $1/\xi_K$ vanishes, and the correlation function remains oscillatory with a slower decay of the envelope function. The position of minima and maxima are interchanged. The analytical calculation of the correlation function provides an excellent understanding of our numerical TD-NRG data.

Remarkably, we have found a building up of correlation even outside of the light-cone for ferromagnetic and antiferromagnetic Kondo couplings in our TD-NRG data. We were able to trace back these correlations to the intrinsic entanglement of the Fermi sea using a second-order perturbation expansion in the Kondo coupling. The analytical structure of the perturbative contribution

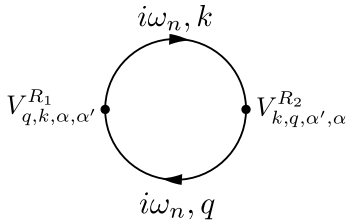


FIG. 13. The second-order Feynman diagram generating the lowest order contribution to the RKKY interaction between to localised spins mediated by a spin excitation propagating through the metallic host.

provide an explanation of the differences observed between ferromagnetic and antiferromagnetic Kondo couplings.

One can see from the structure of the response function, which describes the measurement of a signal at distance R provided a perturbation has been switch on locally at the origin that the commutator structure of linear response function cuts off any correlations outside of the light-cone. Therefore, the correlation function inves-

tigated here does not violate relativity since no information can be transported via these intrinsic correlations.

ACKNOWLEDGMENTS

We would like to acknowledge fruitful discussions with S. Kehrein and M. Medvedyeva. This work was supported by the Deutsche Forschungsgemeinschaft under AN 275/7-1, and supercomputer time was granted by the NIC, FZ Jülich under project No. HHB00.

Appendix A: RKKY-interaction

In this section of the appendix, we briefly summarise how the effective RKKY-interaction between two impurities mediated by a single conduction band is calculated in second order in J .

The interaction between the conduction band electrons and the impurities can be expanded in even (e) and odd (o) parity states [31, 33] and is given by

$$H_{\text{int}} = \frac{J}{8} \sum_{\sigma,\sigma'} \int \int d\epsilon d\epsilon' \sqrt{\rho(\epsilon)\rho(\epsilon')} \vec{\sigma}_{\sigma,\sigma'} \left[\left(\vec{S}_1 + \vec{S}_2 \right) \left(N_e(\epsilon)N_e(\epsilon')c_{\epsilon\sigma,e}^\dagger c_{\epsilon'\sigma',e} + N_o(\epsilon)N_o(\epsilon')c_{\epsilon\sigma,o}^\dagger c_{\epsilon'\sigma',o} \right) + \left(\vec{S}_1 - \vec{S}_2 \right) \left(N_e(\epsilon)N_o(\epsilon')c_{\epsilon\sigma,e}^\dagger c_{\epsilon'\sigma',o} + h.c. \right) \right]. \quad (\text{A1})$$

The normalization factors $\sqrt{\rho(\epsilon)N_{e/o}(\epsilon)}$ have been defined by Eq. (17) in 1D, by (18) in 2D and by (19) in 3D. The RKKY-interaction is generated by a propagation of spin excitation in the conduction band between the two impurities. The leading second order contribution to the RKKY-interaction is depicted as a Feynman diagram in Fig. 13. Integrating out the conduction electrons leads to the effective RKKY interaction H_{RKKY}

$$H_{\text{RKKY}} = \frac{1}{\beta} \sum_{i\omega} \int \int d\epsilon d\epsilon' \sum_{\alpha,\alpha'} G^0(\omega_n, \epsilon) G^0(\omega_n, \epsilon') \cdot V_{\alpha,\alpha'}^{\vec{R}_1}(\epsilon, \epsilon') V_{\alpha',\alpha}^{\vec{R}_2}(\epsilon', \epsilon), \quad (\text{A2})$$

which is exact in second order in J . The vertex operator $V_{\alpha,\alpha'}^{\vec{R}_i}(\epsilon, \epsilon')$ at the position \vec{R}_i , of the impurity spin \vec{S}_i originates from the Hamiltonian H_{int} in (A1) and is defined as

$$V_{\alpha,\alpha'}^{\vec{R}_i}(\epsilon, \epsilon') = c_{p,p'}^i \frac{J}{8} \sqrt{\rho(\epsilon)\rho(\epsilon')} N_p(\epsilon) N_{p'}(\epsilon') \vec{\sigma}_{\sigma,\sigma'} \vec{S}_i \quad (\text{A3})$$

and depends on the combined spin-parity index

$\alpha = (\sigma, p)$ with spin σ and parity p , and the sign factor

$$c_{p,p'}^i = \begin{cases} -1 & \text{if } p \neq p' \text{ and } i = 2 \\ 1 & \text{otherwise} \end{cases}. \quad (\text{A4})$$

$G^0(\omega_n, k) = [i\omega_n - \epsilon_k + i\delta]^{-1}$ denotes the Green's function of a free electron, $i\omega_n$ the fermionic Matsubara frequencies. The textbook [43] evaluation of summation over the Matsubara frequencies yields

$$\frac{1}{\beta} \sum_{i\omega} G^0(\omega_n, \epsilon) G^0(\omega_n, \epsilon') = \frac{f(\epsilon) - f(\epsilon')}{\epsilon - \epsilon'} \quad (\text{A5})$$

where $f(\epsilon)$ labels the Fermi-Dirac distribution. For $T = 0$ and a particle-hole symmetric conduction band, we arrive at

$$H_{\text{RKKY}} = \sum_{\alpha,\alpha'} \int_{-D}^0 d\epsilon \int_0^D d\epsilon' \left(\frac{V_{\alpha,\alpha'}^{R_1}(\epsilon, \epsilon') V_{\alpha',\alpha}^{R_2}(\epsilon', \epsilon)}{\epsilon - \epsilon'} + \frac{V_{\alpha,\alpha'}^{R_2}(\epsilon, \epsilon') V_{\alpha',\alpha}^{R_1}(\epsilon', \epsilon)}{\epsilon - \epsilon'} \right). \quad (\text{A6})$$

After performing the spin and parity summations we ob-

tain the effective spin-spin interaction

$$H_{\text{RKKY}} = \int_{-D}^0 d\epsilon \int_0^D d\epsilon' \rho(\epsilon)\rho(\epsilon') \frac{J^2}{16} \left(\frac{N_e^2(\epsilon)N_e^2(\epsilon') + N_o^2(\epsilon)N_o^2(\epsilon')}{\epsilon - \epsilon'} - \frac{N_e^2(\epsilon)N_o^2(\epsilon') + N_o^2(\epsilon)N_e^2(\epsilon')}{\epsilon - \epsilon'} \right) \vec{S}_1 \vec{S}_2 \quad (\text{A7})$$

which defines the effective RKKY interaction constant K_{RKKY} as

$$K_{\text{RKKY}} = \int_{-D}^0 d\epsilon \int_0^D d\epsilon' \rho(\epsilon)\rho(\epsilon') \frac{J^2}{16} \left(\frac{N_e^2(\epsilon)N_e^2(\epsilon') + N_o^2(\epsilon)N_o^2(\epsilon')}{\epsilon - \epsilon'} - \frac{N_e^2(\epsilon)N_o^2(\epsilon') + N_o^2(\epsilon)N_e^2(\epsilon')}{\epsilon - \epsilon'} \right) \quad (\text{A8})$$

which implicitly depend on the distance via the energy-dependent parity densities $N_e(\epsilon)$ and $N_o(\epsilon)$. If their energy dependence is replaced by a constant $\sqrt{\rho(\epsilon)}N_p(\epsilon) = \rho_0 N_p$, the approximation of Jones and Varma [31]

$$\frac{K_{\text{RKKY}}}{D} = -\frac{J^2 \rho_0^2}{16} 2 \ln(2) (N_e^2 - N_o^2)^2 \quad (\text{A9})$$

is recovered. This K_{RKKY} , however, remains ferromagnetic for all distances R and is insufficient to account for the correct spatial dependent RKKY interaction. As pointed out by Affleck and coworkers [33], maintaining the energy dependency is crucial for the alternating ferromagnetic and antiferromagnetic interaction between two impurity spins as function of increasing distance.

Appendix B: Perturbative approach of spin-spin correlation function $\chi(\vec{r}, t)$

We divide the Hamiltonian into two parts $H = H_0 + H_K$ with $H_0 = \sum_{\sigma, \vec{k}} \varepsilon_{\vec{k}} c_{\vec{k}\sigma}^\dagger c_{\vec{k}\sigma}$, with the free

conduction band dispersion $\varepsilon_{\vec{k}}$ and $H_K = J \vec{S}_{\text{imp}} \vec{s}_c(0)$.

The time-dependent spin-correlation function $\chi(\vec{r}, t) = \langle \vec{S}_{\text{imp}} \vec{s}(\vec{r}) \rangle(t)$ can be calculated

$$\langle \vec{S}_{\text{imp}} \vec{s}(\vec{r}) \rangle(t) = \text{Tr} \left[\rho^I(t) \vec{S}_{\text{imp}} \vec{s}^I(\vec{r}, t) \right] \quad (\text{B1})$$

using density operator $\rho^I(t)$ in the interaction picture, which is defined for any operator A as

$$A^I(t) = e^{iH_0 t} A e^{-iH_0 t} \quad (\text{B2})$$

Since the impurity spin commutes with H_0 , it remains time independent. The real-time evolution of $\rho^I(t)$ can be derived from the von-Neumann equation

$$\partial_t \rho^I(t) = i [\rho^I(t), H_K^I(t)] \quad (\text{B3})$$

which is integrated to

$$\rho^I(t) = \rho_0 + i \int_0^t [\rho_0, H_K^I(t_1)] dt_1 - \int_0^t \int_0^{t_1} [[\rho^I(t_2), H_K^I(t_2)], H_K^I(t_1)] dt_2 dt_1 \quad (\text{B4})$$

using the boundary condition $\rho^I(0) = \rho_0$. For an approximate solution in $O(J^2)$, we replace $\rho^I(t_2)$ by ρ_0 in the second integral. Substitution (B4) into (B1) and cyclically rotate the operators under the trace yields

$$\begin{aligned} \langle \vec{S}_{\text{imp}} \vec{s}(\vec{r}) \rangle(t) &\approx \text{Tr} \left[\rho_0 \vec{S}_{\text{imp}} \vec{s}_I(\vec{r}, t) \right] \\ &+ i \int_0^t \text{Tr} \left[\rho_0 \left[H_K^I(t_1), \vec{S}_{\text{imp}} \vec{s}_I(\vec{r}, t) \right] \right] dt_1 \\ &- \int_0^t \int_0^{t_1} \text{Tr} \left[\rho_0 \left[H_K^I(t_2), \left[H_K^I(t_1), \vec{S}_{\text{imp}} \vec{s}_I(\vec{r}, t) \right] \right] \right] dt_2 dt_1 \end{aligned} \quad (\text{B5})$$

containing only expectation values which only involves the initial density operator ρ_0 in which the impurity spin and the conduction electrons factorise. In the absence of a magnetic field the first term vanishes, and the initial correlation function is zero at $t = 0$. The integral kernel of the first order correction is given by

$$\text{Tr} \left[\rho_0 \left[H_K^I(t_1), \vec{S}_{\text{imp}} \vec{s}_I(\vec{r}, t) \right] \right] = -\frac{3}{4} \frac{J}{V_u N^2} \sum_{\vec{k}, \vec{q}} f(\varepsilon_{\vec{k}+\vec{q}}) \sin \left(\vec{q} \vec{r} + (\varepsilon_{\vec{k}+\vec{q}} - \varepsilon_{\vec{k}})(t_1 - t) \right) \quad (\text{B6})$$

For a linear dispersion in 1D, the argument of the sine contains $(\varepsilon_{\vec{k}+\vec{q}} - \varepsilon_{\vec{k}}) = v_F q$ contributions. The kernel

remains phase coherent on the light-cone $q(r - v_F t)$ and, therefore, generates the response on this light-cone line.

Calculating the commutator of the second order yields

$$\begin{aligned}
\text{Tr} \left[\rho_0 \left[H_K^I(t_2), \left[H_K^I(t_1), \vec{S}_{\text{imp}}^I(\vec{r}, t) \right] \right] \right] &= \frac{3}{8} \frac{J^2}{V_u N^3} \sum_{\vec{k}, \vec{q}_1, \vec{q}_2} f(\epsilon_{\vec{k}+\vec{q}_1}) f(-\epsilon_{\vec{k}-\vec{q}_2}) \times \\
&\left(\cos \left[\vec{q}_1 \vec{r} + (\epsilon_{\vec{k}+\vec{q}_1} - \epsilon_{\vec{k}-\vec{q}_2}) t_1 + (\epsilon_{\vec{k}-\vec{q}_2} - \epsilon_{\vec{k}}) t_2 + (\epsilon_{\vec{k}} - \epsilon_{\vec{k}+\vec{q}_1}) t \right] \right. \\
&+ \cos \left[\vec{q}_2 \vec{r} + (\epsilon_{\vec{k}+\vec{q}_1} - \epsilon_{\vec{k}-\vec{q}_2}) t_1 + (\epsilon_{\vec{k}} - \epsilon_{\vec{k}+\vec{q}_1}) t_2 + (\epsilon_{\vec{k}-\vec{q}_2} - \epsilon_{\vec{k}}) t \right] \\
&- \cos \left[(\vec{q}_1 + \vec{q}_2) \vec{r} - (\epsilon_{\vec{k}+\vec{q}_1} - \epsilon_{\vec{k}-\vec{q}_2}) t - (\epsilon_{\vec{k}-\vec{q}_2} - \epsilon_{\vec{k}}) t_2 - (\epsilon_{\vec{k}} - \epsilon_{\vec{k}+\vec{q}_1}) t_1 \right] \\
&\left. - \cos \left[(\vec{q}_1 + \vec{q}_2) \vec{r} - (\epsilon_{\vec{k}+\vec{q}_1} - \epsilon_{\vec{k}-\vec{q}_2}) t - (\epsilon_{\vec{k}} - \epsilon_{\vec{k}+\vec{q}_1}) t_2 - (\epsilon_{\vec{k}-\vec{q}_2} - \epsilon_{\vec{k}}) t_1 \right] \right) . \tag{B7}
\end{aligned}$$

Because of the simple sine and cosine structure the time integration can be obtained analytically. For the momentum integrations over \vec{k} , \vec{q}_1 and \vec{q}_2 we insert a 1D linear dispersion for $\epsilon_{\vec{k}}$. If we expand (B6) and (B7) for

small times around $t = 0$ the momentum integrations can also be calculated analytically otherwise a numerical integration has to be performed.

-
- [1] J. Kondo, Prog. Theor. Phys **32**, 37 (1964); J. Phys. Soc. Jpn. **74**, 1 (2005).
- [2] W. de Haas, J. de Boer, and G. van den Berg, Physica **1**, 1115 (1934).
- [3] H. C. Manoharan, C. P. Lutz, and D. M. Eigler, Nature **403**, 512 (2000).
- [4] O. Agam and A. Schiller, Phys. Rev. Lett. **86**, 484 (2001).
- [5] G. A. Fiete, J. S. Hersch, E. J. Heller, H. C. Manoharan, C. P. Lutz, and D. M. Eigler, Phys. Rev. Lett. **86**, 2392 (2001).
- [6] D. Goldhaber-Gordon, H. Shtrikman, D. Mahalu, D. Abusch-Magder, U. Meirav, and M. Kastner, Nature **391**, 156 (1998).
- [7] M. A. Kastner, Rev. Mod. Phys. **64**, 849 (1992).
- [8] H. Park, J. Park, A. K. L. Lim, E. H. Anderson, A. P. Alivisatos, and P. L. McEuen, Nature **407**, 57 (2000).
- [9] L. H. Yu and D. Natelson, Nanotechnology **15**, S517 (2004); L. H. Yu, Z. K. Keane, J. Ciszek, L. Cheng, J. M. Tour, T. Baruah, M. R. Pederson, and D. Natelson, Phys. Rev. Lett. **95**, 256803 (2005).
- [10] R. Temirov, A. Lassise, F. B. Anders, and F. S. Tautz, Nanotechnology **19**, 065401 (2008).
- [11] K. G. Wilson, Rev. Mod. Phys. **47**, 773 (1975).
- [12] R. Bulla, T. A. Costi, and T. Pruschke, Rev. Mod. Phys. **80**, 395 (2008).
- [13] P. Schlottmann, Physics Rep. **181**, 1 (1989).
- [14] T. A. Costi, Phys. Rev. B **55**, 3003 (1997).
- [15] P. Nordlander, M. Pustilnik, Y. Meir, N. S. Wingreen, and D. C. Langreth, Phys. Rev. Lett. **83**, 808 (1999).
- [16] J. Paaske, A. Rosch, and P. Wölfle, Phys. Rev. B **69**, 155330 (2004).
- [17] F. B. Anders and A. Schiller, Phys. Rev. Lett. **95**, 196801 (2005); Phys. Rev. B **74**, 245113 (2006).
- [18] S. Kehrein, Phys. Rev. Lett. **95**, 056602 (2005).
- [19] M. Schiró and M. Fabrizio, Phys. Rev. B **79**, 153302 (2009).
- [20] P. Werner, T. Oka, and A. J. Millis, Phys. Rev. B **79**, 035320 (2009).
- [21] H. Schoeller, Eur. Phys. J. Special Topics **168**, 179 (2009); M. Pletyukhov and H. Schoeller, Phys. Rev. Lett. **108**, 260601 (2012); D. Schuricht and H. Schoeller, Phys. Rev. B **80**, 075120 (2009).
- [22] M. Medvedyeva, A. Hoffmann, and S. Kehrein, Phys. Rev. B **88**, 094306 (2013).
- [23] V. Barzykin and I. Affleck, Phys. Rev. B **57**, 432 (1998).
- [24] I. Affleck and P. Simon, Phys. Rev. Lett. **86**, 2854 (2001).
- [25] E. S. Sørensen and I. Affleck, Phys. Rev. Lett. **94**, 086601 (2005).
- [26] I. Affleck, L. Borda, and H. Saleur, Phys. Rev. B **77**, 180404 (2008).
- [27] L. Borda, Phys. Rev. B **75**, 041307 (2007).
- [28] V. Barzykin and I. Affleck, Phys. Rev. Lett. **76**, 4959 (1996).
- [29] E. H. Lieb and D. W. Robinson, Communications in Mathematical Physics **28**, 251 (1972).
- [30] C. Jayaprakash, H. R. Krishna-murthy, and J. W. Wilkins, Phys. Rev. Lett. **47**, 737 (1981).
- [31] B. A. Jones and C. M. Varma, Phys. Rev. Lett. **58**, 843 (1987).
- [32] B. A. Jones, C. M. Varma, and J. W. Wilkins, Phys. Rev. Lett. **61**, 125 (1988).
- [33] I. Affleck, A. W. W. Ludwig, and B. A. Jones, Phys. Rev. B **52**, 9528 (1995).
- [34] A. C. Hewson, *The Kondo Problem to Heavy Fermions* (Cambridge Press, Cambridge UK, 1993).
- [35] In order to avoid different numerical accuracy for $R = 0$ and $R > 0$ calculations, we have used $k_F R / \pi = 0.01$ in the NRG calculations for $R \rightarrow 0$.
- [36] F. B. Anders, Phys. Rev. Lett. **101**, 066804 (2008).
- [37] S. Schmitt and F. B. Anders, Phys. Rev. B **81**, 165106 (2010); Phys. Rev. Lett. **107**, 056801 (2011).
- [38] A. Jovchev and F. B. Anders, Phys. Rev. B **87**, 195112 (2013).
- [39] E. Eidelstein, A. Schiller, F. Güttge, and F. B. Anders, Phys. Rev. B **85**, 075118 (2012).
- [40] F. Guettge, F. B. Anders, U. Schollwoeck, E. Eidelstein, and A. Schiller, Phys. Rev. B **87**, 115115 (2013).
- [41] M. Yoshida, M. A. Whitaker, and L. N. Oliveira,

- Phys. Rev. B **41**, 9403 (1990).
- [42] For a true two-channel calculation using the the same NRG parameters requires a finite R , otherwise $N_o(\varepsilon) = 0$ and the numerics breaks down.
- [43] G. Mahan, *Many-Particle Physics* (Plenum Press, New York, 1981).